Science of the Total Environment 865 (2023) 161286

Contents lists available at ScienceDirect

Science of the Total Environment

journal homepage: www.elsevier.com/locate/scitotenv

The role of dissolved pyrogenic carbon from biochar in the sorption of As (V) in biogenic iron (oxyhydr)oxides

Matheus B. Soares [a,b,*], Owen W. Duckworth [b], Luís R.F. Alleoni [a]

[a] Department of Soil Science, Luiz de Queiroz College of Agriculture (ESALQ), University of São Paulo (USP), 13418900 Piracicaba, SP, Brazil
[b] Department of Crop and Soil Sciences, North Carolina State University, 27695 Raleigh, NC, USA

HIGHLIGHTS

- The dissolved organic carbon (DOC) did not change the binding mechanism of As (V).
- The As(V) was predominantly sorbed in the BIOS as bidentate binuclear complex.
- The pyrolysis temperature played an important role in the DOC quality.
- DOC and As(V) competitive sorption was affected by the pyrolysis temperature.

GRAPHICAL ABSTRACT

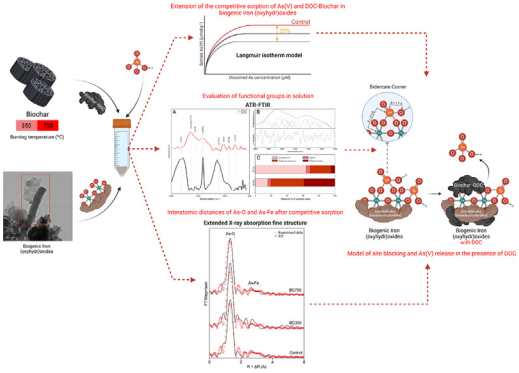

ARTICLE INFO

Editor: Filip M.G. Tack

Keywords:
Biogenic oxides
Bidentate complexes
Biominerals
Dissolved organic carbon
X-ray absorption spectroscopy

ABSTRACT

Water contamination by arsenic (As) affects millions of people around the world, making techniques to immobilize or remove this contaminant a pressing societal need. Biochar and iron (oxyhydr)oxides [in particular, biogenic iron (oxyhydr)oxides (BIOS)] offer the possibility of stabilizing As in remediation systems. However, little is known about the potential antagonism in As sorption generated by the dissolved organic carbon (DOC) from biochar, or whether DOC affects how As(V) interacts with BIOS. For this reason, our objectives were to evaluate the *i*) As (V) sorption potential in BIOS when there is presence of DOC from pyrolyzed biochars at different temperatures; and *ii*) identify whether the presence of DOC alters the surface complexes formed by As(V) sorbed in the BIOS. We conducted As(V) sorption experiments with BIOS at circumneutral pH conditions and in the presence of DOC from sugarcane (*Saccharum officinarum*) straw biochar at pyrolyzed 350 (BC350) and 750 °C (BC750). The As(V) content was quantified by inductively coupled plasma mass spectrometry, and the BIOS structure and As(V) sorption mechanisms were investigated by X-ray absorption spectroscopy. In addition, the organic moieties comprising the DOC from biochars were investigated by attenuated total reflectance Fourier transform infrared spectroscopy. The addition of DOC did not change the biomineral structure or As(V) oxidation state. The presence of DOC, however, reduced by 25 % the sorption of As(V), with BC350 being responsible for the greatest reduction in As(V) sorption capacity. Structural modeling revealed As(V) predominantly formed binuclear bidentate surface complexes on BIOS. The presence of DOC did not change the binding mechanism of As(V) in BIOS, suggesting that the reduction of As(V) sorption to BIOS was due to site blocking. Our results bring insights into the fate of As(V) in surface waters and provide a basis for understanding the competitive sorption of As(V) in environments with biochar application.

* Corresponding author at: Department of Soil Science, Luiz de Queiroz College of Agriculture (ESALQ), University of São Paulo (USP), 13418900 Piracicaba, SP, Brazil.
E-mail address: bortolanza@usp.br (M.B. Soares).

http://dx.doi.org/10.1016/j.scitotenv.2022.161286
Received 11 October 2022; Received in revised form 22 December 2022; Accepted 26 December 2022
Available online 30 December 2022

1. Introduction

Arsenic (As) is a critical naturally occurring contaminant due to its potential toxicity, causing negative health outcomes such as birth defects, neurological problems, cancer, and diabetes (Bundschuh et al., 2022; Genchi et al., 2022). It is estimated that >200 million people in at least 105 countries are at potential risk of As poisoning due to continued ingestion of As contaminated water (Podgorski and Berg, 2020). In the US, the As ranks first on the Agency for Toxic Substances and Disease Registry's list of hazardous substances (Bundschuh et al., 2022).

Due to the health problems caused by exposure to As, there is a critical societal need to develop sustainable technologies and management strategies to immobilize or remove As from water. Both Fe(III) (oxyhydr)oxides (Aftabtalab et al., 2022; Chen et al., 2022; Huan et al., 2022; Sowers et al., 2021) and biochar (Lima et al., 2022; Soares et al., 2022; Yang et al., 2021) have been identified as potential low cost, high affinity sorbents for use in water treatment or remediation. Among the Fe(III) (oxyhydr)oxides studied, there is increasing recognition of bacteriogenic Fe(III) (oxyhydr)oxides (BIOS) commonly found in sediments, and natural waters can play an important role in the sorption of several potential inorganic contaminants (Field et al., 2019; Sowers et al., 2017; Whitaker et al., 2018; Whitaker and Duckworth, 2018). The BIOS have important structural differences, such as low crystallinity, high surface area, incorporation of organic matter, and reduced crystalline domain size (Whitaker et al., 2021), attributes that can result in reactivity and sorption capacity superior to that of synthetic iron (oxyhydr)oxides sorbents.

Biochar is commonly used sorbent because is a sustainable and renewable product with the potential to sorb various organic and inorganic contaminants from soil and natural waters (Cheng et al., 2021; Yoon et al., 2020; Kirmizakis et al., 2022). However, biochar also may release low molecular weight organic compounds that are dissolved and/or suspended in water (DOC) (Li et al., 2018; Soares et al., 2022), potentially affect the sorption of inorganic anions (such as arsenate) to Fe(III) (oxyhydr)oxides through competitive sorption. The release capacity and quality of DOC from biochar are mainly related to feedstock and pyrolysis conditions. As compared to high temperature pyrolysis, low pyrolysis temperatures produce biochar with a greater amount of DOC with a larger proportion of humic compounds (Gui et al., 2020).

The pyrolysis process selects highly stable organic compounds resistant to thermal degradation and at the same time alters the carbon structure, resulting in a graphene-like end product (Elkhalifa et al., 2022; Wang et al., 2022). These physicochemical changes result in biochar with high resistance to biochemical degradation, high surface area, and low DOC release capacity, resulting in a promising sorbent for soil and water remediation (Uras et al., 2012). The amount of DOC that can be released from biochar and interact with BIOS is an important factor for studying competitive sorption because the organic molecules can competition for sorption sites at the mineral surface (Essington, 2003).

Despite the potential of BIOS and biochar as As sorbents, no studies have examined the competition of As(V) and DOC from biochar for sorption in BIOS, resulting in a significant gap in our knowledge. Understanding the secondary effects of biochar, such as the release of DOC into the environment, is essential to assess the effectiveness of remediation and investigate As transport in environments with a strong presence of BIOS. Therefore, the authors' objectives were to: *i*) determine the potential sorption of As(V) in BIOS when there is the presence of DOC from pyrolyzed biochars at different temperatures; and *ii*) identify if the presence of DOC alters the surface complexes formed by As(V) sorbed in BIOS.

2. Materials and methods

2.1. Environmental BIOS sampling

The BIOS sample was collected from the Lake Raleigh dam in Raleigh, North Carolina, USA (35° 45′ 55″ N, 78° 40′ 37″ W; EA Fig. A.1). This site has a perennial occurrence of biofilms containing Fe(III) minerals (Field et al., 2019). Submerged "fluffy" dark orange biomineral assemblage was collected from 3 cm from the water surface using syringes, and transferred repeatedly to 500 mL polypropylene bottles. The pH of the water was 6.9 ± 0.2 at the time of sampling. All BIOS sampling was performed at the same location to reduce the effects of varying environmental conditions such as pH, light, and dissolved oxygen.

After the sampling, the BIOS suspensions were transferred into 50 mL polypropylene centrifuge tubes and centrifuged at 10,000 $\times g$ (RCF) for 10 min in the laboratory. After the supernatant was decanted, the remaining sample was vortexed and mixed with other BIOS samples. This BIOS stock sample was stored in the freezer (storage details are provided in the EA).

2.2. Characterization of the BIOS

The Fe content in the BIOS was extracted with sodium citrate-bicarbonate-dithionite (Klute, 1965) and determined by Flame Atomic Absorption Spectroscopy (FAAS; iCE 3300 AA Spectrophotometer, ThermoFisher Scientific). In addition to Fe, the C and N contents were determined by total combustion using a LECO CN928 Series Macro Determinator analyzer (Sowers et al., 2017). For quality control of the analysis of C and N, the mass of each subsample was weighed within the interval where there is maximum combustion of the sample (up to 50 mg), with function verifies with reference samples provided by the equipment manufacturer.

The morphology, surface, and phase properties of the BIOS were also evaluated. The BIOS samples were imaged by using a variable pressure scanning electron microscope (VPSEM; Hitachi SU3900) and a transmission electron microscope (TEM; Talos F200X, ThermoFisher Scientific).

X-ray diffraction (XRD) was conducted to obtain the crystalline phases present in the BIOS using a Smart Lab Rigaku X-ray Diffractometer with a graphite monochromator operated at 40 kV and 44 mA with Cu Kα radiation (0.1540 nm). After obtaining the diffractograms, the positions, smoothing, and normalization of the diffractogram were performed using Origin 2017 software (OriginLab Corporation, Northampton, Massachusetts, USA). Crystalline phases were identified by *d*-spacing using the HighScore Plus PANalytical software (Malvern PANalytical, Malvern, United Kingdom).

The BIOS surface charge was estimated by ζ-potential analysis. The BIOS samples were diluted in 0.01 M $NaNO_3$ with a final pH of 6.9 ± 0.1 and concentration of 1 g L^{-1}. The samples were loaded into capillary cells and further analyzed in Malvern Zetasizer Nano Z. Malvern's external standard was also evaluated, with a potential of −42 ± 4.2 mV. The specific surface area (SSA) of the BIOS was determined by N_2 sorption (BET isotherm) using a Quantachrome Monosorb surface analyzer (Whitaker and Duckworth, 2018). Additional details about Fe, VPSEM, and TEM analysis are provided in EA.

2.3. Biochar production

The biochar was produced from sugarcane (*Saccharum officinarum*) straw collected after harvest from an agricultural field in Brazil. The choice of sugarcane straw to produce biochar is due to the abundance of this residue (Martíni et al., 2020) and its potential use in bioenergy (Cherubin et al., 2021). The biochars were produced by pyrolysis in a double sealed reactor (without oxygen) with a heating rate of 5 °C min^{-1}, and final pyrolysis temperatures were 350 (BC350) and 750 °C (BC750). The choice of pyrolysis temperatures was due to the physicochemical changes that temperature can provide to the biochar, such as changes in aromatic and aliphatic carbon (Guo et al., 2021; Liu et al., 2021) contents, which can affect the sorption capacity of As by iron oxides.

The elemental composition of the biochar ($n = 3$) was determined according to the EPA method 3051A (USEPA, 2007) (EA Table A.1). Carbon and nitrogen contents were determined by combustion using an elemental analyzer (LECO 828 Series Combustion - Shimadzu). The ash and fixed carbon contents were determined by the muffle method (ASTM, 2007). For the

analysis, the ceramic crucibles were washed with 9.5 % HCl and then dried. Samples were placed in the preheated at 750 °C furnace for 10 min, and then transferred to the desiccator where they remained until cooled. The attribute content was calculated by the difference in mass before and after heating.

The SSA of the biochar ($n = 3$) was determined by the N_2 sorption method, and then the data were adjusted by the BET isotherm (Soares et al., 2022). The biochar characterization data were compared by *Bootstrap* ($p < 0.05$) (Bai et al., 2022), and the choice of the non-parametric mean comparison test was due to the non-normality of the biochar data. More details on biochar production and characterization can be found in Soares et al. (2022).

2.4. DOC extraction and characterization

The DOC of biochar ($n = 3$) was extracted according to the Analytical Methods Guide for Biochar (Singh et al., 2017). Samples with 5 g of biochar were stirred in 50 mL of deionized water (1:10 *w/v*) on a horizontal shaker for 1 h at 21 ± 2 °C. After shaking, the samples were centrifuged and filtered through a 0.22 μm nylon filter. The DOC content, the pH, and the concentrations of NO_3^-, PO_4^{3-} and SO_4^{2-} in the filtrate were determined. The DOC content was quantified using an elemental TOC analyzer (TOC-L, Shimadzu). The NO_3^- and PO_4^{3-} contents were determined by using Latchat Quikchem 8500 (Hauser et al., 1988), whereas SO_4^{2-} was determined by using a Dionex 2000i/sp Ion Chromatograph (Morales et al., 2000).

The absorbance corresponding to the DOC aromaticity ($SUVA_{254}$) was determined by using a Flame-S-UV–vis miniature spectrophotometer equipped with a DH-mini UV–Vis–NIR Deuterium-Halogen Light Source (OceanOptics). The $SUVA_{254}$ (L mg^{-1} m^{-1}) was calculated by Eq. (1):

$$SUVA_{254} = \frac{a254}{DOC} \quad (1)$$

where a254 is the absorption coefficient at the wavelength of 254 nm, DOC is the dissolved organic carbon (mg L^{-1}), and $SUVA_{254}$ is the DOC aromaticity index. The difference in the DOC content and aromaticity index between the biochars was compared by the *Bootstrap* test ($p < 0.05$).

The organic functional groups present in DOC were determined by attenuated total reflectance-Fourier transform infrared spectroscopy (ATR-FTIR, Alpha Bruker). The solution samples were diluted to the same carbon concentration (6.56 mg L^{-1}) to enable the semi-quantification of organic functional groups. A deionized water (blank) was used to calibrate the background spectrum of the ATR-FTIR. For the blank, the pH was corrected to the average pH of each treatment, in order to avoid possible protonation or deprotonation of possible functional groups present in the water.

The data ($n = 4$) were obtained by a reflectance spectrum of 500 to 4000 cm^{-1} with 2 cm^{-1} of resolution. The spectra (32 scans) were averaged, background subtracted and corrected for atmospheric interferences (water vapor and CO_2) using the OPUS/Mentor software. The spectra were preprocessed by the Savitzky-Golay smoothing method, with a 10-point polynomial to reduce electronic and natural oscillations. Finally, the data were normalized to 0 and 1 to improve the visualization of the spectra.

The semiquantitative estimate of the functional groups present in the solution was obtained by integrating the area under the vibrational band at 1800–900 cm^{-1}. The baseline was fitted as a straight line between 1800 and 900 cm^{-1}, and the area under the peak was determined by the 2nd derivative and spectral deconvolution using the Origin 2020 software package (Northampton, Massachusetts, USA). Briefly, after baseline, the spectrum of the 2nd derivative was determined to find the position and the number of bands of structural components.

Once the positions of the peaks were identified and the baseline plotted, Gaussian peaks were added to the band according to the position evidenced by the spectrum of the 2nd derivative. The width and height of the peaks were automatically adjusted in Origin, and the criterion used in the adjustment was the Levenberg-Marquardt interaction algorithm, in which the algorithm minimizes the square of the residual sum of both the adjusted and the experimental spectra (Soares et al., 2022).

The bands represent functional groups that characterize DOC and are less influenced by the O—H vibration of water molecules. The band from 1660 to 1580 cm^{-1} represents aromatic groups (double bond C) (Demyan et al., 2012) whereas the band at 1550–1500 cm^{-1} represents aliphatic groups (CH_2 and CH_3) present in alkanes (Dhillon et al., 2017). The 1440–1395 cm^{-1} band represents C—OO^- vibrations present in carboxylic structures (Peltre et al., 2017). Finally, the 1160–1000 cm^{-1} band is related to C—O—C vibrations associated with polysaccharides (Dhillon et al., 2017). After the integration of the peak areas referring to the band of each of these structures, the results were presented according to their relative contribution (%) to the total area of each spectrum.

2.5. As(V) adsorption isotherms

To evaluate the potential sorption of As(V) in BIOS and the effects of DOC on the competition for specific sorption sites, As(V) sorption isotherms were obtained after a laboratorial sorption experiment performed in suspensions of 2 g L^{-1} BIOS in 50 mL polypropylene centrifuge tubes. Both the As(V) stock solution (500 mg L^{-1}, made with $Na_2HAsO_4{\cdot}7H_2O$ (Sigma-Aldrich)) and the BIOS suspensions were adjusted to pH 6.9 ± 0.1 using NaOH and HCl. The DOC content used in the sorption isotherm was 6.56 mg L^{-1}, with the DOC concentration choice based on the potential of BIOS to sorb As(V) (Sowers et al., 2017). The difference in NO_3^-, PO_4^{3-}, and SO_4^{2-} content between the DOC of the biochars was corrected by addition of $NaNO_3$, Na_3PO_4, and Na_2SO_4 (ThermoFisher Scientific).

BIOS samples with As(V) solution were loaded on an MX RD Pro rotary mixer (DLAB Scientific) for 48 h, and this equilibration time was chosen based on previous studies with BIOS (Sowers et al., 2017; Whitaker et al., 2018; Whitaker and Duckworth, 2018). Samples were checked for pH change using the Orion Star A111 pH meter (ThermoFisher Scientific) and adjusted as necessary to pH 6.9 ± 0.1 After 48 h of agitation, the BIOS samples were centrifuged at 10,000 ×*g* (RCF) for 10 min, passed through a 0.22 μm syringe filter (nylon), and stored at 4 °C in a refrigerator for later analysis. All samples from this experiment were performed in triplicate.

The As content in the solution was determined by Inductively Coupled Plasma Mass Spectrometry (ICP-MS; NexION 300D, PerkinElmer), and ICP-MS with a quadrupole system was used to avoid the polyatomic interference of ArCl. The content of As sorbed in BIOS was calculated by the difference between the concentrations of As in solution before and after sorption. The sorption data was modeled to a Langmuir isotherm using preprogrammed an Excel spreadsheet with a non-linear solver (Bolster and Hornberger, 2007). The criteria for choosing the model (Freundlich, Freundlich-Langmuir, Langmuir, and Two-surface Langmuir models) were the sum of squared errors, Akaike's Information Criterion, and model efficiency.

2.6. X-ray absorption spectroscopy

The K-edge XAS spectra of As and Fe were collected at room temperature (~25 °C) in fluorescence mode at the Stanford Synchrotron Radiation Lightsource (SSRL) on beamlines 11–2 and 4–3, respectively. On beamline 11–2, the incident beam was adjusted using a Si(220) $\phi = 90°$ variable output dual crystal monochromator, where the energy was selected with a monochromator Si(111) $\phi = 90°$ at beamline 4–3. Spectra were collected by using a PIPS detector equipped with Soller slits and a Z-1 X-ray filter (Ge or Mn) to improve the signal-to-noise ratio. The energies were calibrated by adjusting the E_0 to the Au L-edge of an Au foil and the Fe K-edge of a Fe foil.

The As and Fe K-edge spectra were energy calibrated, averaged, and background corrected using the SIXPACK interface (Webb, 2005), which makes use of the IFEFFIT code (Newville, 2001). Linear combination fitting of Fe XANES and normalized Fe EXAFS was conducted in SIXPACK using Fe (III) mineral standards to elucidate the phase and structure of the BIOS

(Harrington et al., 2012; Liu and Hesterberg, 2011). Components that contributed <5 % of the spectral reconstruction were removed and fitting recalculated using the remaining defaults. A list of all standards considered in the adjustments is available in the electronic annex (EA Table A.2).

To elucidate if DOC altered the As(V) sorption mechanisms in the BIOS, structural fitting (shell-by-shell) was performed on the As EXAFS spectra using the SIXPACK software. Pathways were generated using the Angelellite mineral $[Fe^{3+}{}_4(AsO_4)_2O_3]$ (Bolanz et al., 2013) in FEFF9 (Rehr et al., 2010). The threshold energy correction factor (E_0) and Debye-Waller parameter (σ^2) were allowed to optimize but were linked to a common value for all shells. The amplitude reduction factor (S_0^2) was set at 0.85 (Foster et al., 1998; Paktunc et al., 2003; Sowers et al., 2017).

The spectra were modeled using a first As—O shell (R ≈ 1.7 Å) and a second shell containing monodentate (R ≈ 2.8 Å) and bidentate (R ≈ 3.3 Å) binuclear As—Fe complexes (Gao et al., 2013). In both shells, the parameter N was fixed R was allowed to float, and f was used to determine the fraction of monodentate complexes in the second shell (Sowers et al., 2017). However, fits to our spectra were not improved by the inclusion of a monodentate As—Fe complex path, as determined by significance testing at the 95 % confidence interval (Hamilton, 1965). Therefore, the final fit model was composed of a first shell containing an As—O scattering path and a second shell containing one As—Fe path.

3. Results and discussion

3.1. BIOS properties

The BIOS sample contained 13.5 % Fe (*w*/w), 5.71 % C (w/w), 0.6 % N (w/w), with a C:N ratio of 9.45. The Fe and C contents found in the BIOS were within the range of the BIOS dataset previously investigated at different times and regions in North Carolina, USA (6.3–43 % and 2.7–15 % (w/w), respectively) (Almaraz et al., 2017; Field et al., 2019; Sowers et al., 2017; Whitaker et al., 2021, 2018; Whitaker and Duckworth, 2018). It is worth noting that Fe content has been shown to be directly related to surface area and inversely proportional to C content in a study of 38 BIOS samples (Field et al., 2019).

The morphology and spatial distributions of C, Fe, and Ti were characterized in VPSEM-EDS images (EA Fig. A.2). Most of the BIOS surface was composed of Fe and C, indicating the formation of a binary phase composed mainly of Fe and C. There was greater homogeneity in the distribution of Fe when compared to C and Ti (which focus on hotspots). In addition, the EDS spectra in three regions of the BIOS (EA. Fig. A.3) showed the presence and homogeneous distribution of Si on the sample surface, this element being later present as quartz in the XRD analysis (EA Fig. A.4) and possibly as an incorporated cation in Hydrous Fe(III) oxide, as seen in the XAS analysis (Fig. 3). Transmission electron micrographs showed irregular filamentous structures (EA Fig. A.2H), similar to those observed in other Fe(III) microbial mats (Chan et al., 2009).

The crystalline phases of the BIOS were identified using XRD and XAS approaches. In diffractograms (EA Fig. A.4), the main crystalline phases containing Fe identified in the BIOS were 2-line ferrihydrite, and possibly goethite. The normalized Fe K-edge XANES and EXAFS linear combination fits (Table 2 and Fig. 3) showed that the BIOS is composed of poorly ordered Fe(III) minerals such as hydrated Fe(III) oxide with silicon, 2-line ferrihydrite, and a Fe(III) carboxylate complex. Beyond Fe minerals, XRD also indicated the presence of quartz and kaolinite. With the exception of the possible identification of goethite, these phases are consistent with those previously found in BIOS (Sowers et al., 2019, 2017; Whitaker et al., 2021, 2018; Whitaker and Duckworth, 2018).

The ζ-potential revealed an electrokinetic potential of −18.5 mV, indicating a predominance of negative charge at pH below 7. This result suggests that the organic phase present in the BIOS plays an important role in reducing the zero point of charge (ZPC). The presence of negatively charged organic matter incorporated in the BIOS structure has been shown to reduce the ζ-potential of BIOS as compared to ferrihydrite. Our ζ-potential results were more positive than those of Sowers et al. (2017). It is worth noting that BIOS from Sowers et al. (2017) contained almost twice as much C, which suggests greater incorporation of negatively charged organic matter into their BIOS.

The SSA of the BIOS was 85 $m^2\ g^{-1}$, falling within the range of 65 to 312 $m^2\ g^{-1}$ previously reported for BIOS samples (Childs et al., 1982; Cismasu et al., 2011; Ferris et al., 2010; Field et al., 2019; Kennedy et al., 2011; Sowers et al., 2017; Whitaker et al., 2018; Whitaker and Duckworth, 2018). The low SSA of the BIOS in relation to the other Fe (III) oxyhydroxides is due in part to its composition (relatively low %Fe and high %C). Fe has been found to positive correlate with surface area whereas C has been shown to correlate negatively (Field et al., 2019). The SSA of organic carbon is generally low (~1 $m^2\ g^{-1}$) (Chiou et al., 1990) while Fe(III) minerals such as ferrihydrite have an SSA of 200 to 350 $m^2\ g^{-1}$ due to the absence of OC and the high content of phases containing Fe(III) oxide (Field et al., 2019; Jambor and Dutrizac, 1998; Sowers et al., 2017).

3.2. Investigating the chemistry of dissolved organic carbon

The pyrolysis temperature altered not only the elemental composition of the biochar (EA Table A.1) but also the amount and the quality of the DOC of the biochar (EA Table A.3 and Fig. 1). Notably, high temperature BC750 produced 51 % less DOC than BC350. This change in the biochar composition and DOC quantity is caused by the physicochemical changes that carbon compounds undergo during the thermal process of pyrolysis (Xing et al., 2021).

The structure of DOC also may vary with pyrolysis temperature. The ATR-FTIR spectra of DOC showed that the overall absorbance was different between BC350 and BC750, with relatively little spectral information above 2000 cm^{-1} (Fig. 1A). The DOC of the biochars had a pronounced absorbance from 1800 to 1000 cm^{-1}, with the absorbance bands assigned to compounds representing aromatic groups (double bond C) aliphatic groups (CH_2 and CH_3) present in alkanes, C—OO^- vibrations present in carboxylic structures, and finally, C—O—C associated with polysaccharides (Demyan et al., 2012; Dhillon et al., 2017; Peltre et al., 2017).

The difference in absorbance between BC350 and BC750 stems from varying proportions of aromatic C═C, alkane, carboxylates, and polysaccharides (Fig. 1C). Considering that the DOC's ATR-FTIR analysis was performed for BC350 and BC750 under similar conditions of pH and DOC concentrations, the intensities and widths of the bands may reflect the relative concentrations of these moieties. The presence of more aromatic compounds in BC750, which is also observed in the $SUVA_{254}$ obtained by UV–vis (EA Table A.3), can be explained by the thermochemical transformations generated by the burning of the feedstock. At high pyrolysis temperatures (~700 °C), compounds with low thermal resistance are converted into CO_2, leaving only highly stable compounds such as aromatic compounds with C═C bond (Tomczyk et al., 2020; Yi et al., 2022). More sensitive compounds such as sugars and polysaccharides are rapidly degraded (Moldoveanu, 2010).

The proportions of organic groups in the solution can play a key role in understanding competitive sorption with As(V). Sowers et al. (2019) investigated DOM sorption in BIOS and found the BIOS preferential sorption of aromatic and carboxylic species in a manner that was resilient to desorption at high ionic strength. This demonstrates that the presence in quantity and quality of DOC may play an important role in the immobilization of As (V) in circumneutral environments where the BIOS is a sink of this contaminant.

3.3. Sorption of As(V) to BIOS

The As(V) concentration associated with the BIOS surface increased as the dissolved As(V) concentration increased, with decreasing slope at As (V) concentrations above 200 μM (Fig. 2 and EA Fig. A.5). The data showed a nonlinear slope with the presence of concavity in relation to the abscissa, which is consistent with an L-type isotherm, characterized by a decrease in the slope of the curve, as the number of available sites for adsorption

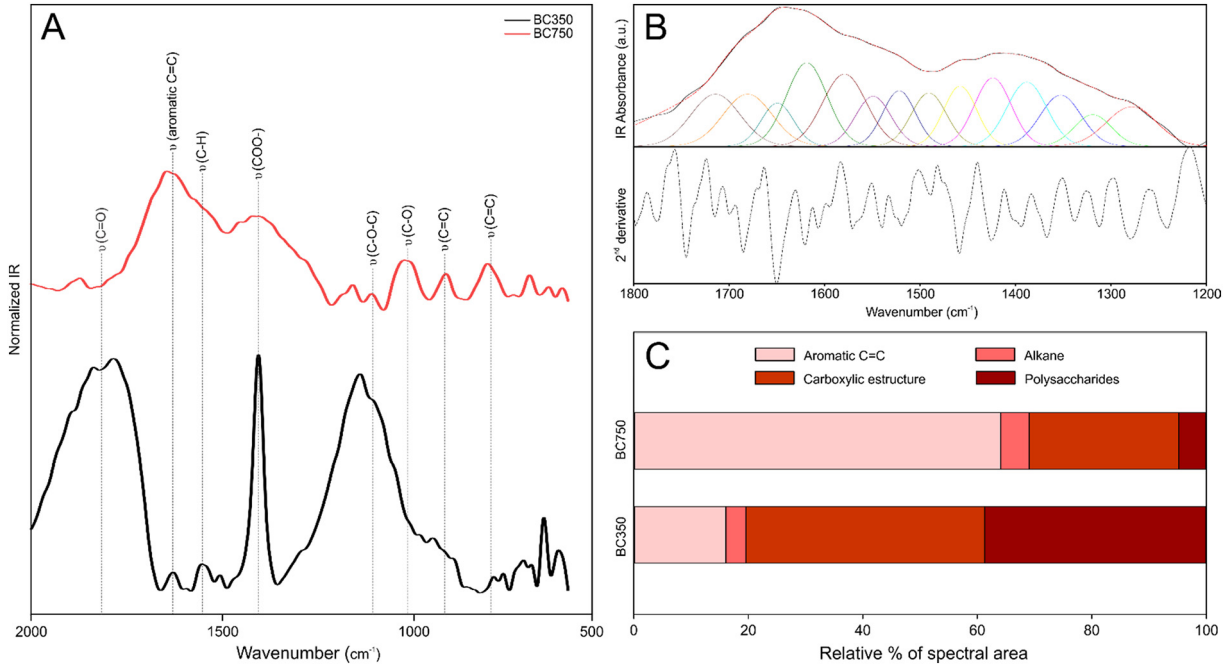

Fig. 1. A = ATR-FTIR spectra of dissolved organic carbon extracted from pyrolyzed biochars at 350 (BC350) and 750 °C (BC750). B = Example of the infrared spectrum analysis process. Bands referring to aromatic, alkanes, carboxylic structures, and polysaccharides were deconvoluted into Gaussian curves at the peak position initially determined by the spectrum of the 2nd derivative of the original data. C = Percent area under ATR-FTIR spectra for regions corresponding to aromatics (1660–1580 cm^{-1}), alkanes (1550–1500 cm^{-1}), carboxylic structures (1440–1395 cm^{-1}), and polysaccharides (1160–1000 cm^{-1}). Relative % of spectral area refers to the relative percentage of the integrated area of aromatic, alkanes, carboxylic structures, and polysaccharides in the total area of the spectrum.

decreases, due to the covering of the adsorbent surface. It indicates that, at low concentrations, the surface has a high affinity for the adsorbed substance, and this affinity decreases at higher concentrations (Sposito, 2008).

The As(V) sorption normalized by BIOS mass showed a difference in sorption when DOC was present (Table 1). The maximum As(V) sorbed in BIOS was 186 μmol g^{-1} while, in the presence of DOC, this value reduced to 131 and 150 μmol g^{-1} for BC350 and BC750, respectively (Table 1). The concentration of As(V) sorbed in the BIOS in the absence of DOC (186 μmol g^{-1}) is below the content found by Sowers et al. (2017), Dixit and Hering (2003), and Pierce and Moore (1982). However, when normalized by specific surface area, our BIOS had sorption of 2.2 μmol m^{-2}, a value within the average (2.0–2.4 μmol m^{-2}) of the BIOS evaluated by Sowers et al. (2017) and near the value (2.5 μmol m^{-2}) found by Dixit and Hering for ferrihydrite (2003). The differences in the values may be due to differences in experimental conditions between studies.

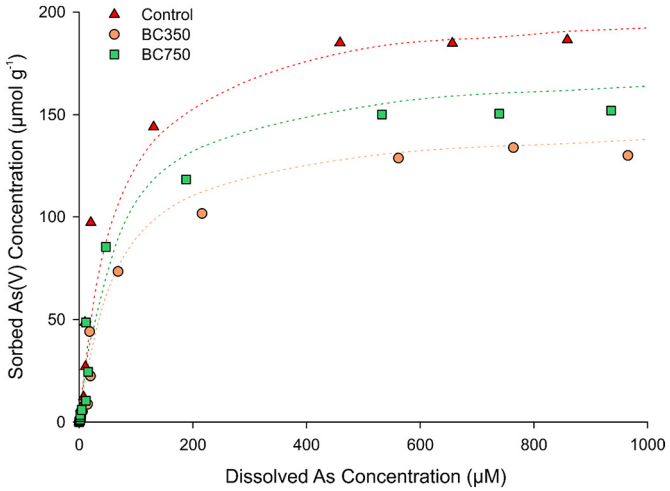

Fig. 2. Mass-normalized sorption of As(V) sorption to biogenic iron (oxyhydr)oxide. All data were modeled using the Langmuir sorption isotherm model, with fit parameters shown in Table 1.

A reduction between 20 and 30 % was observed in the BIOS ability to sorb As(V) when DOC was present. The difference in As(V) sorption in BC350 and BC750 may be related to the quality of DOC such as its molecular weight and aromaticity. Minerals rich in surface hydroxyl groups, such as iron (oxyhydr)oxides, can preferentially sorb organic compounds of high molecular weight dissolved or suspended in solution (Grybos et al., 2009).

Besides the preference of Fe(III) minerals for sorbing higher molecular weight compounds, the carbon structure may be fundamental for the preferential sorption in BIOS. BC350 has a greater amount of carboxylic structure (Fig. 1C), which may have a greater affinity to sorb on BIOS. According to Sowers et al. (2019), BIOS preferentially sorbs aromatic and carboxylic species with concomitant enrichment in the solution of aliphatic groups not associated with carboxylic acids, which suggests that part of the DOC of the biochar may be interacting with the inorganic and organic phases of the BIOS, resulting in the release of biomolecules from the BIOS that were present during the neogenesis of this mineral. It is worth noting that the LCF of Fe K-edge XANES shows a trend of increasing contribution of Fe(III)-carboxylate complexes from the control to high and low

Table 1
Langmuir parameters used to model As(V) sorption to biogenic iron (oxyhydr)oxide samples normalized to mass. Q_{max} = maximum sorption capacity; K_L = Langmuir's isothermal constant; E = model efficiency on the scale 0 to 1.

Data set[a]	Q_{max} (μmol g^{-1})	K_L (L μmol $^{-1}$)	E
Control	187 ± 8	0.028 ± 0.002	0.942
BC350	131 ± 5	0.018 ± 0.002	0.892
BC750	150 ± 6	0.024 ± 0.001	0.950

[a] Control = biogenic iron (oxyhydr)oxide without dissolved organic carbon (DOC) from biochar, BC350 = biogenic iron (oxyhydr)oxide with DOC from biochar pyrolyzed at 350 °C, and BC750 = biogenic iron (oxyhydr)oxide with DOC from biochar pyrolyzed at 750 °C.

Table 2
Linear combination fit results for biomineral samples using X-ray absorption spectroscopy data. The linear combination adjustment was performed in SIXPACK software and normalized to 100 %, with raw adjustments adding up to 100 ± 0.15 % for the XANES spectra and 100 ± 12 % for the EXAFS spectra. Uncertainty is reported as the software output but is estimated at 5 %.

Sample[a]	Standard	% contribution	R-factor
XANES spectra linear combination fits			
Control	Ferrihydrite	60 ± 0.2	0.00003
	Fe(III)-Rhiz	16 ± 0.2	
	Hydrous Fe(III) oxide with Si	24 ± 0.1	
BC350	Ferrihydrite	55 ± 0.2	0.00002
	Fe(III)-Rhiz	30 ± 0.2	
	Hydrous Fe(III) oxide with Si	15 ± 0.1	
BC750	Ferrihydrite	55 ± 0.2	0.00002
	Fe(III)-Rhiz	27 ± 0.1	
	Hydrous Fe(III) oxide with Si	18 ± 0.1	
EXAFS spectra linear combination fits			
Control	Ferrihydrite	67 ± 8	0.016
	Fe(III)-Rhiz	5 ± 2	
	Hydrous Fe(III) oxide with Si	35 ± 9	
BC350	Ferrihydrite	74 ± 8	0.016
	Fe(III)-Rhiz	5 ± 2	
	Hydrous Fe(III) oxide with Si	30 ± 9	
BC750	Ferrihydrite	71 ± 8	0.016
	Fe(III)-Rhiz	5 ± 2	
	Hydrous Fe(III) oxide with Si	36 ± 9	

[a] BC350 = biogenic iron (oxyhydr)oxide with DOC from biochar pyrolyzed at 350 °C, and BC750 = biogenic iron (oxyhydr)oxide with DOC from biochar pyrolyzed at 750 °C. Control is biogenic iron (oxyhydr)oxides without the addition of DOC. Fe(III)-Rhiz = Fe(III)-rhizoferrin (carboxylate complex).

temperature DOC treatments, but this trend is not seen in the corresponding EXAFS LCF (Table 2).

3.4. BIOS structure and As(V) sorption mechanism

Changes in BIOS structure with DOC addition were probed by Fe K-edge XAS. Excerpt for the previously mentioned trend in organic complexes in the XANES fits, results are consistent between samples, particularly for EXAFS fits (Table 2 and Fig. 3B). A superposition of the control and the DOC EXAFS in *k*-space is shown in EA Fig. A.6 to emphasize the similarity of the spectra. Thus, XAS results suggest that BIOS did not undergo significant structural change in response to DOC exposure.

The EXAFS spectrum for As is shown in Fig. 4 and the shell-by-shell fitting results are shown in Table 3. For all treatments, the first As—O shell fixed coordination numbers were close to the expected values for As (V) (Das et al., 2014; Gao et al., 2013; Sherman and Randall, 2003; Sowers et al., 2017; Voegelin et al., 2007; Waychunas et al., 1993). In the FTs of the As spectra, a large peak at R = 1.7 Å is characteristic of the As—O bond distance. These results, which are consistent with XANES spectra that show a peak center aligned with an As(V) standard around 11,875 eV, suggest that the As present on the BIOS surface remains in its initial oxidation state, evidencing that the BIOS and DOC did not reduce As(V) to As (III).

The EXAFS spectra also showed the smaller peaks seen at R larger than the first shell distance, which can be interpreted as coming from Fe scattering or multiple scattering phenomena (Sowers et al., 2017). In all three spectra, the second shell was best fit with a peak at near R = 3.3 Å (Fig. 5). This distance has been suggested to indicate the presence of

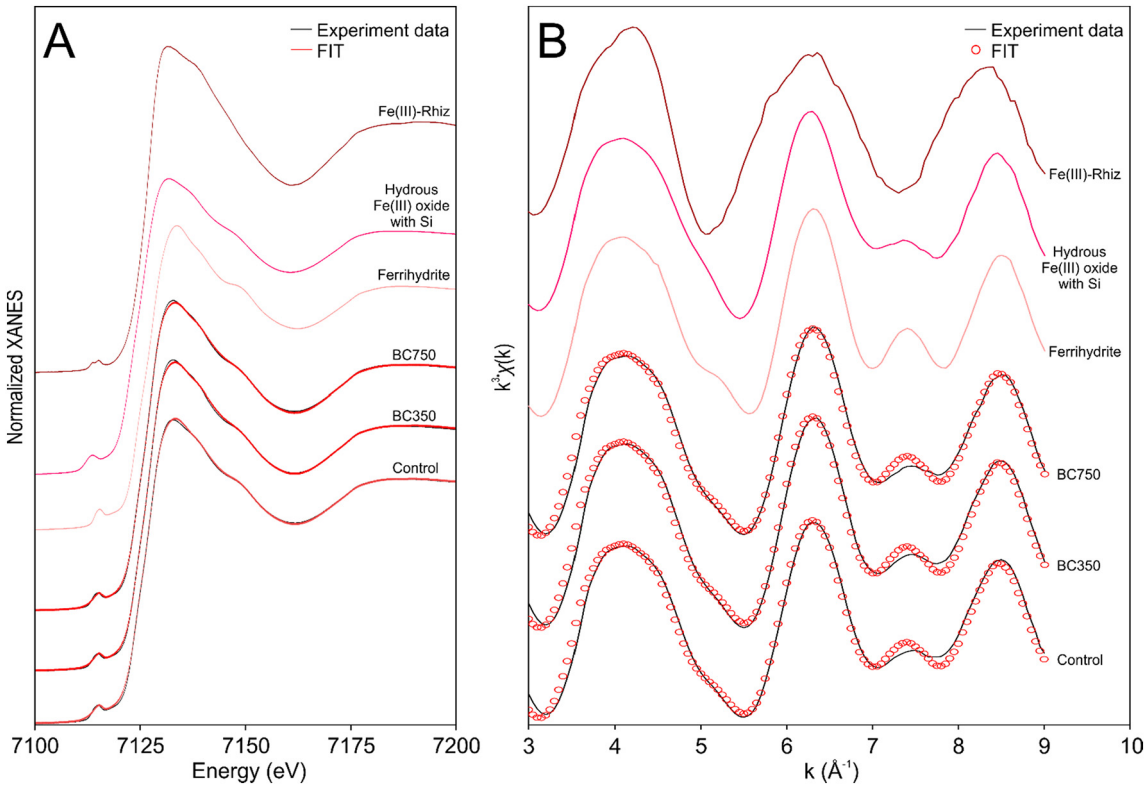

Fig. 3. Fe K-edge spectra (A) XANES and (B) EXAFS for biogenic iron (oxyhydr)oxides samples and Fe(III) standards. The solid lines in B represent the k^3-weighted χ(k)-spectra, and the circles and red dotted lines (in A) represent the best fits obtained with the linear combination fitting. The fit parameters are shown in Table 2. BC350 and BC750 are biogenic iron (oxyhydr)oxides amended with dissolved organic carbon from pyrolyzed biochar at 350 and 750 °C, respectively. Control refers to non-amended biogenic iron (oxyhydr)oxides. (For interpretation of the references to color in this figure legend, the reader is referred to the web version of this article.)

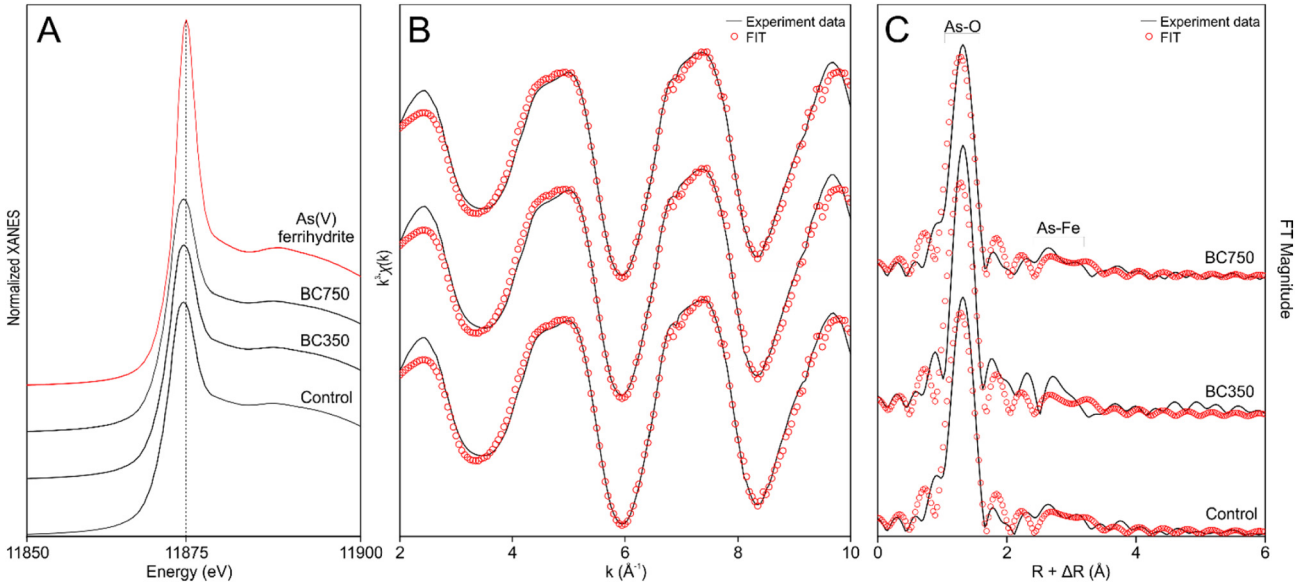

Fig. 4. As K-edge (A) XANES, (B) EXAFS spectra, and (C) FT magnitude for biogenic iron (oxyhydr)oxides samples used in sorption isotherm experiment. Solid lines represent the k^3-weighted χ(k)-spectra (B) and Fourier transform spectra in R space (C), and the red circles represent the best fits obtained with structural models shown in Table 3. BC350 and BC750 are biogenic iron (oxyhydr)oxides amended with dissolved organic carbon from pyrolyzed biochar at 350 and 750 °C, respectively. Control refers to non-amended biogenic iron (oxyhydr)oxides. (For interpretation of the references to color in this figure legend, the reader is referred to the web version of this article.)

bidentate binuclear coordination of As(V) on BIOS and ferrihydrite (Gao et al., 2013; Sowers et al., 2019).

As(V) sorbs predominantly through a bidentate binuclear complex with sharing electrons with Fe(III) in the corner of the crystal structure (Waychunas et al., 1993; Gao et al., 2013). Although previously identified in hematite (Catalano et al., 2008), we did not evaluate the possibility outer-sphere complexes (Fukushi and Sverjensky, 2007) in this study owing to the difficulty in identifying them in EXAFS data in the presence of inner spectra complexes. Furthermore, our data also cannot exclude the possibility of ternary complexes systems with DOC.

The interatomic distance between As and Fe did not change after the addition of DOC. This consistency indicates that the presence of DOC and the pyrolysis temperature of the biochar did not affect the As(V) sorption mechanism in the BIOS. This difference between As(V) sorption with and without DOC is thus likely due to the competition of As(V) and organic anions to sorb on the BIOS surface. Namely, DOC can occupy sorption sites on the surface of the Fe(III) minerals and thus reduce the sorption of As (V) (Bauer and Blodau, 2006). Therefore, it is possible to conclude that DOC has preference to sorb in the BIOS, reducing the As(V) sorption by up to 25 % without changing the binding mechanisms.

It is known that DOC can affect As mobilization by complexation or competition for sorption sites on mineral oxides (Aftabtalab et al., 2022). It is expected that DOC sorption on Fe(III) minerals is simultaneously controlled by multiple mechanisms in acidic and neutral media, including mainly "surface ligand exchange", "hydrophobic force" and "van der Waals forces" models (Wu et al., 2008). On the other hand, the sorption of As(V) in Fe(III) minerals initially occurs by electrostatic interactions in free edges of $Fe(O, OH)_6$ towards octahedral chains (Manceau, 1995).

The presence of DOC can reduce the density of positive charge on the surface of Fe(III) minerals, making electrostatic interactions between

Table 3
Coordination numbers, interatomic distances, and Debye–Waller factors for As sorbed onto biogenic iron (oxyhydr)oxides.

	As-O			As-Fe bidentate		
	N[g]	*R* (Å)	σ^2 (Å^2)	N[g]	*R* (Å)	σ^2 (Å^2)
Control	4	1.70 ± 0.01	0.0013 ± 0.0008	2	3.31 ± 0.05	0.008 ± 0.006
BC350[h]	4	1.70 ± 0.02	0.0008 ± 0.0012	2	3.32 ± 0.09	0.009 ± 0.010
BC750	4	1.70 ± 0.01	0.0013 ± 0.0007	2	3.31 ± 0.05	0.009 ± 0.006
As(V)-Ferrihydrite[a]	3.20 ± 0.60	1.68 ± 0.01	0.0010 ± 0.002	1 ± 3	3.31 ± 0.05	0.01 ± 0.01
Low As(V)-EnvFe[a]	3.70 ± 0.70	1.68 ± 0.01	0.0010 ± 0.001	1 ± 3	3.30 ± 0.05	0.01 ± 0.01
High As(V)-EnvFe[a]	3.50 ± 0.70	1.67 ± 0.01	0.0010 ± 0.001	2 ± 3	3.29 ± 0.05	0.01 ± 0.01
As(V)-Ferrihydrite[b]	4.00	1.680	0.00290	1.3	3.27	0.0042
As(V)-Ferrihydrite[c]	4.00	1.670	0.02000	1.8	3.30	0.01
As(V)-Ferrihydrite[d]	3.79	1.663	0.03500	2.57	3.26	0.011
As(V)-Ferrihydrite[e]	4.00	1.690	0.00290	2.0	3.27	0.0061
As(V)-Ferrihydrite[f]	4.05	1.690	0.00260	2.0	3.31	0.0103

[a] Sowers et al. (2017).
[b] Gao et al. (2013).
[c] Sherman and Randall (2003).
[d] Waychunas et al. (1993).
[e] Das et al. (2014).
[f] Voegelin et al. (2007).
[g] Represents the fixed parameters: $S_0^2 = 0.85$ (Sowers et al. (2017); Foster et al., 1998; Paktunc et al., 2003); and $N = 4$ and 2.
[h] BC350 = biogenic iron (oxyhydr)oxide with DOC from biochar pyrolyzed at 350 °C, and BC750 = biogenic iron (oxyhydr)oxide with DOC from biochar pyrolyzed at 750 °C. Control is biogenic iron (oxyhydr)oxides without the addition of DOC.

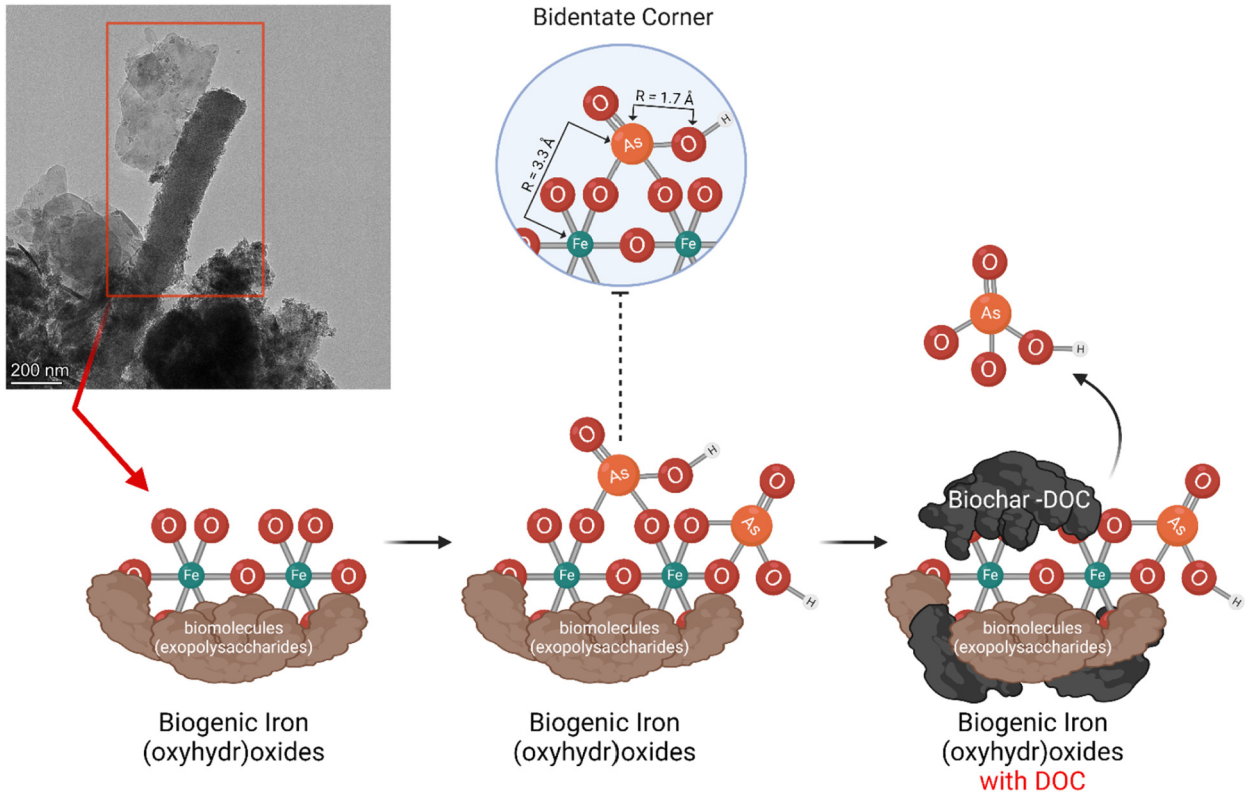

Fig. 5. Model of site blocking and As(V) release in the presence of dissolved organic carbon from biochar. The model was based on EXAFS As and Fe data, shell-by-shell fitting of As—O and bidentate As—Fe shell, and sorption isotherm study. Data were verified by previously published coordination numbers and interatomic distances (Das et al., 2014; Sherman and Randall, 2003; Sowers et al., 2017; Voegelin et al., 2007; Waychunas et al., 1993). Our data do not exclude the possibility that part of As(V) remains sorbed on the organic phase on the surface of biogenic iron oxide, nor do they take the contribution of outer-sphere bonds into consideration.

anionic As(V) and positive Fe(III) minerals less favorable (Au et al., 1999; Hunter and Liss, 1982). Furthermore, we speculate that although there was no difference in sorption mechanisms between BC350 and BC750, the changes in As(V) sorbed amount and the difference in DOC quality investigated by ATR-FTIR may indicate that the preferential sorption of compounds carboxylic acid was the predominant factor responsible for the lower As(V) sorption in BC350 treatment. We suggest, as a way of evaluating our speculation about the BIOS preference to sorb suspended or dissolved organic compounds from the biochar, studies that sorption kinetics coupled to a Fourier Transform-Ion-Cyclotron Resonance-Mass spectrometry (FT-ICR-MS) (Sowers et al., 2019).

Although DOC did not change the As(V) sorption mechanism and we did not assess the effect of the environment on competitive As(V) and DOC sorption onto BIOS, we emphasize that environmental changes play a fundamental role in the effectiveness of As(V) sorption onto BIOS. Changes in pH and Eh can increase the availability of DOC and reduce the sorption capacity of As(V) (Mensah et al., 2022), as well as promote the biotic and abiotic reduction of As(V) and Fe(III) (An et al., 2022; Razzak et al., 2021), increasing the availability of As in the environment and reducing the effectiveness of the BIOS to sorb this contaminant.

4. Final remarks

Our results confirm previous reports that indicate that BIOS is mineralogically similar to synthetic 2-line ferrihydrite. Furthermore, they suggest that the application of DOC to biochar does not change the Fe(III) structure of BIOS but do not exclude the interaction of DOC with the organic phase of BIOS.

The K-edge As EXAFS analysis demonstrates that the presence of DOC and BIOS does not reduce As(V) to As(III), indicating that the presence of the oxyanion at circumneutral pH remains in its original oxidation state. The K-edge analysis of As(V) EXAFS reveals preferential As(V) sorption to BIOS via binuclear bidentate surface complexes.

The presence of DOC does not alter the binding mechanism of As(V) on the BIOS but reduces the maximum As(V) sorption capacity by up to 25 % in environments contaminated with 1200 μM of As, possibly by competitive adsorption of DOC and blocking the sorption sites. Additionally, the pyrolysis temperature affects only the extent of As(V) sorption, with no differences in the As(V) sorption mechanism or changes in the Fe(III) structure. However, ATR-FTIR analysis coupled with observations from a previous study (Sowers et al., 2019) suggests that the pyrolysis temperature provides distinct organic phases in the solution that prefer to be sorbed on the BIOS surface and thus affect the sorption of As(V).

The application of biochar for water and effluent treatment and for environmental remediation has increased in recent years due to the physicochemical properties of biochar and its advantages over traditional techniques such as ion exchange, membrane separation, chemical precipitation, which are techniques that present high cost and inevitable generation of chemical residue. Our study shows minimal antagonistic interactions between biochar DOC and BIOS, suggesting biochar and BIOS could be used together in designed remediation or water treatment systems.

Fe(III) biominerals can, even when DOC is present, be important regulators of As(V) transport in slow-moving surface waters where the application of biochar may facilitate DOC contact with BIOS. However, biochar can introduce some problems not evaluated in this study, such as limited capacity to sorb As and the possibility of facilitating the desorption of As sorbed in the BIOS due to redox changes in the solution caused by the release of DOC.

We recommend that future studies seek to quantify the extent of the effects of DOC concentration and contact time on the competition with As (V) by sorption in BIOS, in addition to evaluating the degree of As (V) retention through desorption study.

CRediT authorship contribution statement

The manuscript was written through the contributions of all authors. All authors have approved the final version of the manuscript.

Data availability

Data will be made available on request.

Declaration of competing interest

The authors declare that they have no known competing financial interests or personal relationships that could have appeared to influence the work reported in this paper.

Acknowledgments

The 1st author gratefully thanks the São Paulo Research Foundation (FAPESP) (grants #2019/06897-9; 2020/13700-4) and the Brazilian Council for Scientific and Technological Development - Conselho Nacional de Desenvolvimento Científico e Tecnológico (CNPq) (grants #140830/2018-9) for the scholarships granted for this research. This study was partially funded by CNPq and the Coordination for the Improvement of Higher Education Personnel - Coordenação de Aperfeiçoamento de Pessoal de Nível Superior (CAPES) – Finance Code 001. This research was funded in part by the National institute of Environmental Health Sciences (P42ES031007 and P30ES025128). This work was supported by the USDA National Institute of Food and Agriculture, Hatch project NC02713. We also thank Andrew Whitaker, Hannah Peel, Ryan Davis, Erik Nelson, Wayne Robarge, Chucky Mooney, and Toby Tung for their assistance. Part of this work was performed in part at the Environmental and Agricultural Testing Service laboratory (EATS), Department of Crop and Soil Sciences, at North Carolina State University and the Analytical Instrumentation Facility (AIF) at North Carolina State University, which is supported by the State of North Carolina and the National Science Foundation (ECCS-2025064). The AIF is a member of the North Carolina Research Triangle Nanotechnology Network (RTNN), a site in the National Nanotechnology Coordinated Infrastructure (NNCI). Use of the Stanford Synchrotron Radiation Lightsource, SLAC National Accelerator Laboratory, is supported by the U.S. Department of Energy, Office of Science, and Office of Basic Energy Sciences under Contract No. DE-AC02-76SF00515.

Appendix A. Supplementary data

Supplementary data to this article can be found online at https://doi.org/10.1016/j.scitotenv.2022.161286.

References

Aftabtalab, A., Rinklebe, J., Shaheen, S.M., Niazi, N.K., Moreno-Jiménez, E., Schaller, J., Knorr, K.H., 2022. Review on the interactions of arsenic, iron (oxy)(hydr)oxides, and dissolved organic matter in soils, sediments, and groundwater in a ternary system. Chemosphere 286, 131790. https://doi.org/10.1016/J.CHEMOSPHERE.2021.131790.

Almaraz, N., Whitaker, A.H., Andrews, M.Y., Duckworth, O.W., 2017. Assessing biomineral formation by iron-oxidizing bacteria in a Circumneutral Creek. J. Contemp. Water Res. Educ. 160, 60–71. https://doi.org/10.1111/J.1936-704X.2017.03240.X.

An, W., Wu, C., Xue, S., Liu, Z., Liu, M., Li, W., 2022. Effects of biochar/AQDS on As(III)-adsorbed ferrihydrite reduction and arsenic (As) and iron (Fe) transformation: abiotic and biological conditions. Chemosphere 291, 133126. https://doi.org/10.1016/J.CHEMOSPHERE.2021.133126.

ASTM, 2007. ASTM D1762-84 - Standard Test Method for Chemical Analysis of Wood. https://doi.org/10.1520/D1762-84R13.

Au, K.K., Penisson, A.C., Yang, S., O'Melia, C.R., 1999. Natural organic matter at oxide/water interfaces: complexation and conformation. Geochim. Cosmochim. Acta 63, 2903–2917. https://doi.org/10.1016/S0016-7037(99)00268-9.

Bai, S.H., Omidvar, N., Gallart, M., Kämper, W., Tahmasbian, I., Farrar, M.B., Singh, K., Zhou, G., Muqadass, B., Xu, C.Y., Koech, R., Li, Y., Nguyen, T.T.N., van Zwieten, L., 2022. Combined effects of biochar and fertilizer applications on yield: a review and meta-analysis. Sci. Total Environ. 808, 152073. https://doi.org/10.1016/J.SCITOTENV.2021.152073.

Bauer, M., Blodau, C., 2006. Mobilization of arsenic by dissolved organic matter from iron oxides, soils and sediments. Sci. Total Environ. 354, 179–190. https://doi.org/10.1016/J.SCITOTENV.2005.01.027.

Bolanz, R.M., Wierzbicka-Wieczorek, M., Čaplovičová, M., Uhlík, P., Göttlicher, J., Steininger, R., Majzlan, J., 2013. Structural incorporation of As5+ into hematite. Environ. Sci. Technol. 47, 9140–9147. https://doi.org/10.1021/ES305182C/SUPPL_FILE/ES305182C_SI_001.PDF.

Bolster, C.H., Hornberger, G.M., 2007. On the use of linearized langmuir equations. Soil Sci. Soc. Am. J. 71, 1796–1806. https://doi.org/10.2136/SSSAJ2006.0304.

Bundschuh, J., Niazi, N.K., Alam, M.A., Berg, M., Herath, I., Tomaszewska, B., Maity, J.P., Ok, Y.S., 2022. Global arsenic dilemma and sustainability. J. Hazard. Mater. 436, 129197. https://doi.org/10.1016/J.JHAZMAT.2022.129197.

Catalano, J.G., Park, C., Fenter, P., Zhang, Z., 2008. Simultaneous inner- and outer-sphere arsenate adsorption on corundum and hematite. Geochim. Cosmochim. Acta 72, 1986–2004. https://doi.org/10.1016/J.GCA.2008.02.013.

Chan, C.S., Fakra, S.C., Edwards, D.C., Emerson, D., Banfield, J.F., 2009. Iron oxyhydroxide mineralization on microbial extracellular polysaccharides. Geochim. Cosmochim. Acta 73, 3807–3818. https://doi.org/10.1016/J.GCA.2009.02.036.

Chen, M., Liu, Y., Zhang, D., Zhu, J., Chen, X., Yuan, L., 2022. Remediation of arsenic-contaminated paddy soil by iron oxyhydroxide and iron oxyhydroxide sulfate-modified coal gangue under flooded condition. Sci. Total Environ. 804, 150199. https://doi.org/10.1016/J.SCITOTENV.2021.150199.

Cheng, N., Wang, B., Wu, P., Lee, X., Xing, Y., Chen, M., Gao, B., 2021. Adsorption of emerging contaminants from water and wastewater by modified biochar: a review. Environ. Pollut. 273, 116448. https://doi.org/10.1016/J.ENVPOL.2021.116448.

Cherubin, M.R., Bordonal, R.O., Castioni, G.A., Guimarães, E.M., Lisboa, I.P., Moraes, L.A.A., Menandro, L.M.S., Tenelli, S., Cerri, C.E.P., Karlen, D.L., Carvalho, J.L.N., 2021. Soil health response to sugarcane straw removal in Brazil. Ind. Crop. Prod. 163, 113315. https://doi.org/10.1016/J.INDCROP.2021.113315.

Childs, C.W., Downes, C.J., Wells, N., 1982. Hydrous iron oxide minerals with short range order deposited in a spring/stream system, Tongariro National Park, New Zealand. Soil Res. 20, 119–129. https://doi.org/10.1071/SR9820119.

Chiou, C.T., Lee, J.-F., Boyd, S.A., 1990. The surface area of soil organic matter. Environ. Sci. Technol. 24, 1031–1036.

Cismasu, A.C., Michel, F.M., Tcaciuc, A.P., Tyliszczak, T., Brown, G.E., 2011. Composition and structural aspects of naturally occurring ferrihydrite. Compt. Rendus Geosci. 343, 210–218. https://doi.org/10.1016/J.CRTE.2010.11.001.

Das, S., Essilfie-Dughan, J., Hendry, M.J., 2014. Arsenate partitioning from ferrihydrite to hematite: spectroscopic evidence. Am. Mineral. 99, 749–754. https://doi.org/10.2138/AM.2014.4657/MACHINEREADABLECITATION/RIS.

Demyan, M.S., Rasche, F., Schulz, E., Breulmann, M., Müller, T., Cadisch, G., 2012. Use of specific peaks obtained by diffuse reflectance fourier transform mid-infrared spectroscopy to study the composition of organic matter in a haplic chernozem. Eur. J. Soil Sci. 63, 189–199. https://doi.org/10.1111/J.1365-2389.2011.01420.X.

Dhillon, G.S., Gillespie, A., Peak, D., van Rees, K.C.J., 2017. Spectroscopic investigation of soil organic matter composition for shelterbelt agroforestry systems. Geoderma 298, 1–13. https://doi.org/10.1016/J.GEODERMA.2017.03.016.

Dixit, S., Hering, J.G., 2003. Comparison of arsenic(V) and arsenic(III) sorption onto iron oxide minerals: implications for arsenic mobility. Environ. Sci. Technol. 37, 4182–4189. https://doi.org/10.1021/ES030309T/ASSET/IMAGES/LARGE/ES030309TF00006.JPEG.

Elkhalifa, S., Mackey, H.R., Al-Ansari, T., McKay, G., 2022. Pyrolysis of biosolids to produce biochars: a review. Sustainability 14, 9626. https://doi.org/10.3390/SU14159626.

Essington, M.E., 2003. Soil and Water Chemistry: An Integrative Approach. 1st ed. CRC Press, Boca Raton.

Ferris, F.G., Konhauser, K.O., Lyvén, B., Pedersen, K., 2010. Accumulation of Metals by Bacteriogenic Iron Oxides in a Subterranean Environment. 16, pp. 181–192. https://doi.org/10.1080/014904599270677.

Field, H.R., Whitaker, A.H., Henson, J.A., Duckworth, O.W., 2019. Sorption of copper and phosphate to diverse biogenic iron (oxyhydr)oxide deposits. Sci. Total Environ. 697, 134111. https://doi.org/10.1016/J.SCITOTENV.2019.134111.

Foster, A.L., Brown, J., Tingle, T.N., Parks, G.A., 1998. Quantitative arsenic speciation in mine tailings using X-ray absorption spectroscopy. Am. Mineral. 83, 553–568. https://doi.org/10.2138/AM-1998-5-616/MACHINEREADABLECITATION/RIS.

Fukushi, K., Sverjensky, D.A., 2007. A predictive model (ETLM) for arsenate adsorption and surface speciation on oxides consistent with spectroscopic and theoretical molecular evidence. Geochim Cosmochim Acta 71, 3717–3745. https://doi.org/10.1016/J.GCA.2007.05.018.

Gao, X., Root, R.A., Farrell, J., Ela, W., Chorover, J., 2013. Effect of silicic acid on arsenate and arsenite retention mechanisms on 6-L ferrihydrite: a spectroscopic and batch adsorption approach. Appl. Geochem. 38, 110–120. https://doi.org/10.1016/J.APGEOCHEM.2013.09.005.

Genchi, G., Lauria, G., Catalano, A., Carocci, A., Sinicropi, M.S., 2022. Arsenic: a review on a great health issue worldwide. Applied Sciences 12, 6184. https://doi.org/10.3390/APP12126184.

Grybos, M., Davranche, M., Gruau, G., Petitjean, P., Pédrot, M., 2009. Increasing pH drives organic matter solubilization from wetland soils under reducing conditions. Geoderma 154, 13–19. https://doi.org/10.1016/J.GEODERMA.2009.09.001.

Gui, X., Liu, C., Li, F., Wang, J., 2020. Effect of pyrolysis temperature on the composition of DOM in manure-derived biochar. Ecotoxicol. Environ. Saf. 197, 110597. https://doi.org/10.1016/J.ECOENV.2020.110597.

Guo, G., Wang, Q., Huang, Q., Fu, Q., Liu, Y., Wang, J., Hu, S., Mašek, O., Wang, L., Zhang, J., 2021. Effect of pyrolysis temperature on the characterisation of dissolved organic matter from pyroligneous acid. Molecules 26, 3416. https://doi.org/10.3390/MOLECULES26113416.

Hamilton, W.C., 1965. Significance tests on the crystallographic R factor. Acta Crystallogr. 18, 502–510. https://doi.org/10.1107/S0365110X65001081.

Harrington, J.M., Parker, D.L., Bargar, J.R., Jarzecki, A.A., Tebo, B.M., Sposito, G., Duckworth, O.W., 2012. Structural dependence of mn complexation by siderophores: donor group dependence on complex stability and reactivity. Geochim. Cosmochim. Acta 88, 106–119. https://doi.org/10.1016/J.GCA.2012.04.006.

Hauser, P.C., Tan, S.S., Cardwell, T.J., Cattrall, R.W., Hamilton, L.C., 1988. Versatile manifold for the simultaneous determination of ions in flow injection analysis. Analyst 113, 1551–1555. https://doi.org/10.1039/AN9881301551.

Huan, Z., Zhang, J., Guo, P., Lin, Z., Li, J., Li, Z., Zhao, W., Cao, S., Zhu, Y., Zhang, T., 2022. Application of iron oxyhydroxide to stabilize As(V) and phenylarsonic acid in contaminated soil: adsorption and the relevance to bioavailability. Environ. Sci. Pollut. Res. 1, 1–14. https://doi.org/10.1007/S11356-022-20646-8/FIGURES/7.

Hunter, K.A., Liss, P.S., 1982. Organic matter and the surface charge of suspended particles in estuarine waters1. Limnol. Oceanogr. 27, 322–335. https://doi.org/10.4319/LO.1982.27.2.0322.

Jambor, J.L., Dutrizac, J.E., 1998. Occurrence and constitution of natural and synthetic ferrihydrite, a widespread iron oxyhydroxide. Chem. Rev. 98, 2549–2585. https://doi.org/10.1021/CR970105T/ASSET/IMAGES/LARGE/CR970105TF00024.JPEG.

Kennedy, C.B., Gault, A.G., Fortin, D., Clark, I.D., Ferris, F.G., 2011. Retention of Iodide by Bacteriogenic Iron Oxides. 28, pp. 387–395. https://doi.org/10.1080/01490451003653110.

Kirmizakis, P., Tawabini, B., Siddiq, O.M., Kalderis, D., Ntarlagiannis, D., Soupios, P., 2022. Adsorption of Arsenic on Fe-Modified Biochar and Monitoring Using Spectral Induced Polarization. Water 14 (4), 563. https://doi.org/10.3390/W14040563.

Klute, A., 1965. Part 1: physical and mineralogical properties, including statistics of measurement and sampling. Methods of Soil Analysis. Black, C. A., Madison, pp. 1–770.

Li, G., Khan, S., Ibrahim, M., Sun, T.R., Tang, J.F., Cotner, J.B., Xu, Y.Y., 2018. Biochars induced modification of dissolved organic matter (DOM) in soil and its impact on mobility and bioaccumulation of arsenic and cadmium. J. Hazard. Mater. 348, 100–108. https://doi.org/10.1016/J.JHAZMAT.2018.01.031.

Lima, J.Z., Ferreira da Silva, E., Patinha, C., Durães, N., Vieira, E.M., Rodrigues, V.G.S., 2022. Sorption of arsenic by composts and biochars derived from the organic fraction of municipal solid wastes: kinetic, isotherm and oral bioaccessibility study. Environ. Res. 204, 111988. https://doi.org/10.1016/J.ENVRES.2021.111988.

Liu, H., Xu, H., Wu, Y., Ai, Z., Zhang, J., Liu, G., Xue, S., 2021. Effects of natural vegetation restoration on dissolved organic matter (DOM) biodegradability and its temperature sensitivity. Water Res. 191, 116792. https://doi.org/10.1016/J.WATRES.2020.116792.

Liu, Y.T., Hesterberg, D., 2011. Phosphate bonding on noncrystalline Al/Fe-hydroxide coprecipitates. Environ. Sci. Technol. 45, 6283–6289. https://doi.org/10.1021/ES201597J/SUPPL_FILE/ES201597J_SI_001.PDF.

Manceau, A., 1995. The mechanism of anion adsorption on iron oxides: evidence for the bonding of arsenate tetrahedra on free Fe(O, OH)6 edges. Geochim. Cosmochim. Acta 59, 3647–3653. https://doi.org/10.1016/0016-7037(95)00275-5.

Martíni, A.F., Valani, G.P., Boschi, R.S., Bovi, R.C., Simões da Silva, L.F., Cooper, M., 2020. Is soil quality a concern in sugarcane cultivation? A bibliometric review. Soil Tillage Res 204, 104751. https://doi.org/10.1016/j.still.2020.104751.

Mensah, A.K., Marschner, B., Wang, J., Bundschuh, J., Wang, S.L., Yang, P.T., Shaheen, S.M., Rinklebe, J., 2022. Reducing conditions increased the mobilisation and hazardous effects of arsenic in a highly contaminated gold mine spoil. J. Hazard. Mater. 436, 129238. https://doi.org/10.1016/J.JHAZMAT.2022.129238.

Moldoveanu, S.C., 2010. Pyrolysis of Carbohydrates. Techniques and Instrumentation in Analytical Chemistry. Elsevier, pp. 419–470 https://doi.org/10.1016/S0167-9244(09)02816-9.

Morales, J.A., de Graterol, L.S., Mesa, J., 2000. Determination of chloride, sulfate and nitrate in groundwater samples by ion chromatography. J. Chromatogr. A 884, 185–190. https://doi.org/10.1016/S0021-9673(00)00423-4.

Newville, M., 2001. IFEFFIT : interactive XAFS analysis and FEFF fitting. J. Synchrotron Radiat. 8, 322–324. https://doi.org/10.1107/S0909049500016964.

Paktunc, D., Foster, A., Laflamme, G., 2003. Speciation and characterization of arsenic in Ketza River mine tailings using x-ray absorption spectroscopy. Environ Sci Technol 37, 2067–2074. https://doi.org/10.1021/ES026185M/ASSET/IMAGES/LARGE/ES026185MF00008.JPEG.

Peltre, C., Gregorich, E.G., Bruun, S., Jensen, L.S., Magid, J., 2017. Repeated application of organic waste affects soil organic matter composition: evidence from thermal analysis, FTIR-PAS, amino sugars and lignin biomarkers. Soil Biol. Biochem. 104, 117–127. https://doi.org/10.1016/J.SOILBIO.2016.10.016.

Pierce, M.L., Moore, C.B., 1982. Adsorption of arsenite and arsenate on amorphous iron hydroxide. Water Res. 16, 1247–1253. https://doi.org/10.1016/0043-1354(82)90143-9.

Podgorski, J., Berg, M., 2020. Global threat of arsenic in groundwater. Science 1979 (368), 845–850. https://doi.org/10.1126/SCIENCE.ABA1510/SUPPL_FILE/ABA1510_PODGORSKI_SM.PDF.

Razzak, A., Shafiquzzaman, M., Haider, H., Alresheedi, M., 2021. Arsenic removal by iron-oxidizing bacteria in a fixed-bed coconut husk column: experimental study and numerical modeling. Environ. Pollut. 272, 115977. https://doi.org/10.1016/J.ENVPOL.2020.115977.

Rehr, J.J., Kas, J.J., Vila, F.D., Prange, M.P., Jorissen, K., 2010. Parameter-free calculations of X-ray spectra with FEFF9. Phys. Chem. Chem. Phys. 12, 5503–5513. https://doi.org/10.1039/B926434E.

Sherman, D.M., Randall, S.R., 2003. Surface complexation of arsenic(V) to iron(III) (hydr)oxides: structural mechanism from ab initio molecular geometries and EXAFS spectroscopy. Geochim. Cosmochim. Acta 67, 4223–4230. https://doi.org/10.1016/S0016-7037(03)00237-0.

Singh, B., Camps-Arbestain, M., Lehmann, J., 2017. Biochar: A Guide to Analytical Methods. Taylor and. ed. CSIRO, Boca Raton.

Soares, M.B., Cerri, C.E.P., Demattê, J.A.M., Alleoni, L.R.F., 2022. Biochar aging: impact of pyrolysis temperature on sediment carbon pools and the availability of arsenic and lead. Sci. Total Environ. 807, 151001. https://doi.org/10.1016/J.SCITOTENV.2021.151001.

Soares, M.B., Santos, F.H., Alleoni, L.R.F., 2022. Temporal changes in arsenic and lead pools in a contaminated sediment amended with biochar pyrolyzed at different temperatures. Chemosphere 287, 132102. https://doi.org/10.1016/J.CHEMOSPHERE.2021.132102.

Sowers, T.D., Harrington, J.M., Polizzotto, M.L., Duckworth, O.W., 2017. Sorption of arsenic to biogenic iron (oxyhydr)oxides produced in circumneutral environments. Geochim. Cosmochim. Acta 198, 194–207. https://doi.org/10.1016/J.GCA.2016.10.049.

Sowers, T.D., Holden, K.L., Coward, E.K., Sparks, D.L., 2019. Dissolved organic matter sorption and molecular fractionation by naturally occurring bacteriogenic iron (Oxyhydr)oxides. Environ. Sci. Technol. 53, 4295–4304. https://doi.org/10.1021/ACS.EST.9B00540/ASSET/IMAGES/LARGE/ES-2019-00540H_0006.JPEG.

Sowers, T.D., Nelson, C.M., Blackmon, M.D., Jerden, M.L., Kirby, A.M., Diamond, G.L., Bradham, K.D., 2021. Interconnected Soil Iron and Arsenic Speciation Effects on Arsenic Bioaccessibility and Bioavailability: A Scoping Review. 25, pp. 1–22. https://doi.org/10.1080/10937404.2021.1996499.

Sposito, G., 2008. The Chemistry of Soils. 2nd ed. Nova York.

Tomczyk, A., Sokołowska, Z., Boguta, P., 2020. Biochar physicochemical properties: pyrolysis temperature and feedstock kind effects. Rev. Environ. Sci. Biotechnol. 19, 191–215. https://doi.org/10.1007/s11157-020-09523-3.

Uras, Ü., Carrier, M., Hardie, A.G., Knoetze, J.H., 2012. Physico-chemical characterization of biochars from vacuum pyrolysis of south african agricultural wastes for application as soil amendments. J. Anal. Appl. Pyrolysis 98, 207–213. https://doi.org/10.1016/J.JAAP.2012.08.007.

USEPA, 2007. Method 3051A: Microwave Assisted Acid Digestion of Sediments, Sludges, Soils and Oils. EPA, Washington.

Voegelin, A., Weber, F.A., Kretzschmar, R., 2007. Distribution and speciation of arsenic around roots in a contaminated riparian floodplain soil: micro-XRF element mapping and EXAFS spectroscopy. Geochim. Cosmochim. Acta 71, 5804–5820. https://doi.org/10.1016/J.GCA.2007.05.030.

Wang, Y., Srinivasakannan, C., Wang, H., Xue, G., Wang, L., Wang, X., Duan, X., 2022. Preparation of novel biochar containing graphene from waste bamboo with high methylene blue adsorption capacity. Diam. Relat. Mater. 125, 109034. https://doi.org/10.1016/J.DIAMOND.2022.109034.

Waychunas, G.A., Rea, B.A., Fuller, C.C., Davis, J.A., 1993. Surface chemistry of ferrihydrite: part 1. EXAFS studies of the geometry of coprecipitated and adsorbed arsenate. Geochim. Cosmochim. Acta 57, 2251–2269. https://doi.org/10.1016/0016-7037(93)90567-G.

Webb, S.M., 2005. SIXpack: a graphical user interface for XAS analysis using IFEFFIT. Phys. Scripta T. T115, 1011–1014. https://doi.org/10.1238/Physica.Topical.115a01011.

Whitaker, A.H., Austin, R.E., Holden, K.L., Jones, J.L., Michel, F.M., Peak, D., Thompson, A., Duckworth, O.W., 2021. The structure of natural biogenic iron (oxyhydr)oxides formed in circumneutral pH environments. Geochim. Cosmochim. Acta 308, 237–255. https://doi.org/10.1016/J.GCA.2021.05.059.

Whitaker, A.H., Duckworth, O.W., 2018. Cu, Pb, and Zn sorption to biogenic iron (oxyhydr) oxides formed in circumneutral environments. Soil Systems 2, 18. https://doi.org/10.3390/SOILSYSTEMS2020018.

Whitaker, A.H., Peña, J., Amor, M., Duckworth, O.W., 2018. Cr(VI) uptake and reduction by biogenic iron (oxyhydr)oxides. Environ. Sci. Process. Impacts 20, 1056–1068. https://doi.org/10.1039/C8EM00149A.

Wu, H., Lin, Y., Wu, J., Zeng, L., Zeng, D., Du, J., 2008. Surface adsorption of iron oxide minerals for phenol and dissolved organic matter. Earth Sci. Front. 15, 133–141. https://doi.org/10.1016/S1872-5791(09)60013-0.

Xing, J., Xu, G., Li, G., 2021. Comparison of pyrolysis process, various fractions and potential soil applications between sewage sludge-based biochars and lignocellulose-based biochars. Ecotoxicol. Environ. Saf. 208, 111756. https://doi.org/10.1016/J.ECOENV.2020.111756.

Yang, D., Yang, S., Wang, L., Xu, J., Liu, X., 2021. Performance of biochar-supported nanoscale zero-valent iron for cadmium and arsenic co-contaminated soil remediation: insights on availability, bioaccumulation and health risk. Environ. Pollut. 290, 118054. https://doi.org/10.1016/J.ENVPOL.2021.118054.

Yi, Z., Li, C., Li, Q., Zhang, L., Zhang, S., Wang, S., Qin, L., Hu, X., 2022. Influence of CO2 atmosphere on property of biochar from pyrolysis of cellulose. J. Environ. Chem. Eng. 10, 107339. https://doi.org/10.1016/J.JECE.2022.107339.

Yoon, K., Cho, D.W., Bhatnagar, A., Song, H., 2020. Adsorption of As(V) and Ni(II) by Fe-Biochar composite fabricated by co-pyrolysis of orange peel and red mud. Environ Res 188, 109809. https://doi.org/10.1016/J.ENVRES.2020.109809.